J Mater Sci (2006) 41:7261–7271
DOI 10.1007/s10853-006-0421-0

Microstructural mechanisms governing the fatigue failure of polyamide 66 fibres

J. M. Herrera Ramirez · A. R. Bunsell · Ph. Colomban

Received: 3 February 2006 / Accepted: 8 May 2006 / Published online: 28 October 2006

Abstract The tensile and fatigue behaviours of two types of high performance polyamide 66 fibres have been studied. Marked differences have been found in their fatigue behaviours although their simple tensile behaviours were almost identical. The fibres have been analysed by DSC, X-ray diffraction and by Raman spectroscopy. The fibres have been seen to possess different microstructures with different percentages of ordered regions. In addition the compressive stresses in the regions near the surfaces of the fibres have been found to differ markedly, which may explain the existence of a minimum cyclic load threshold for fatigue failure and suggest a method for improving fatigue resistance.

J. M. H. Ramirez · A. R. Bunsell (✉)
Ecole des Mines de Paris, Centre des Matériaux, BP 87, 91003 Evry Cedex, France
e-mail: anthony.bunsell@mat.ensmp.fr

Ph. Colomban
Nanophase and Heterogeneous Solids Group, Laboratoire Dynamique, Interactions et Réactivité UMR 7075 CNRS & UPMC, 2 rue Henry-Dunant, 94320 Thiais, France

Present Address:
J. M. H. Ramirez
Centro de Desarrollo Industrial, Direction General de Industria Militar, Av. Industria Militar 1111, Lomas de Tecamachalco, Naucalpan, Edo. Mexico, Mexico

Introduction

Fatigue failure in thermoplastic fibres was identified more than 30 years ago but the microstructural processes governing such behaviour remain the source of speculation. Polyamide 66, 6, PEN and PET fibres have been shown to share a common fatigue process and as these fibres are often used in industrial structures, for which unforeseen failure should be avoided, a better understanding of the mechanisms involved is desirable. The fatigue process occurs when the cyclic load amplitude is sufficiently large, however, a necessary condition for fatigue failure is that the minimum load each cycle be lower than a threshold stress level. Failure under fatigue conditions leads to distinctive fracture morphologies very different from those seen after tensile or creep failure and this allows easy identification of the fatigue process.

Two types of high tenacity polyamide 66 fibres have been subjected to tensile, creep and fatigue tests. The fibres showed very similar behaviour in tension but a marked difference in fatigue. The cyclic loading conditions leading to a given lifetime with one fibre type had to be raised by approximately 25% with respect to the other fibre type, if a similar lifetime was to be expected. The fracture morphologies obtained in tensile and fatigue tests were identical. This remarkable difference in fatigue strength in two types of fibres, which in simple tensile tests were almost identical, has been used to better understand the fatigue process in these fibres.

The role of the microstructure of the fibres in determining fatigue failure will be discussed in the paper as well as the possibility of improving their resistance to fatigue.

Materials tested and experimental techniques employed

Two types of high performance polyamide 66 fibres have been considered. The fibres were produced by different manufacturers and the details of the processes are not known. However both types of fibre were made for use in tyre cords. The fibres will be referred to in this paper as Fibre PA66-A and Fibre PA66-B. The fibres of both types were cylindrical with usually a smooth surface aspect although Fibre PA66-B exhibited rather more surface defects than Fibre PA66-A but this was not considered to be significant. The fibres differed in average diameters with Fibre PA66-A having a mean diameter of 25.4 μm and the other fibre 27.1 μm and both showed similar variations in diameters when different fibres from the same bundle were examined. Details are given below. All loading conditions applied to the fibres were normalised to their cross-sections.

The diameter of each fibre was measured before each test by using a Mitutoyo LSM-6000 laser apparatus. After calibration, by comparison with results obtained with a scanning electron microscope, the accuracy obtained was ±0.1 μm. The apparatus scanned the fibre with light from a laser and the signal obtained from the light cell was a function of the time that the beam was obscured. The apparatus was used in this study after other techniques had been examined and found to be less precise. The results were obtained in real time and allowed the diameter of the fibre to be measured accurately along its length, if necessary. In the present study three diameter measurements were made along the fibre and the average of the three used to calculate the fibre cross-section and to normalise the applied loads.

The variation of diameter within bundles of the fibres was examined by image analysis. The bundles, comprising 210 monofilaments were embedded in epoxy resin, which was cured at room temperature. The specimens were then cooled with liquid nitrogen and sliced using a microtome controlled by a 2065 Supercut Lica Instruments microprocessor. The cut specimens were then coated with 2.5 nm of gold/palladium, using a Cressington 208HR apparatus, which allowed a very uniform coating to be laid down. Photographs were taken of the sliced specimens using an 800-X magnification in a Zeiss Gemini 982 field emission scanning electron microscope, which had been calibrated using a calibration grill. The contours of the fibres were reconstituted using Adobe Photoshop. The analysis of the image allowed the variations in fibre diameters within the bundles of each type of fibre to be ascertained.

The Zeiss Gemini field emission scanning electron microscope, equipped with a Cameca SX 50 microprobe, was used for all subsequent observations of the fibres and the same coating conditions were used as described above. A beam voltage of 1–3 kV was employed and a working distance of 4 mm was used for the observations. Secondary electron emissions were used to obtain the images.

Mechanical tests were performed on individual monofilaments, called fibres in this paper, using a Universal Fibre Tester [1]. This machine has been described in essence elsewhere but considerable changes have been made to it as compared to the description, which appears in Ref. 1. The machine has been turned on its side so that the fibre is held horizontally in the grips. This allows for easier mounting of the specimens and permits more readily, in other studies, tests at temperature. The mechanical part of the machine, without the electronic controls, is shown in Fig. 1. A Sensotec 250 g load cell, calibrated from 0 to 125 g, with a precision of 0.01 g, was used and allowed both steady and cyclic loading patterns to be monitored. For fatigue tests, the electronic controls monitored both the average and cyclic load patterns,

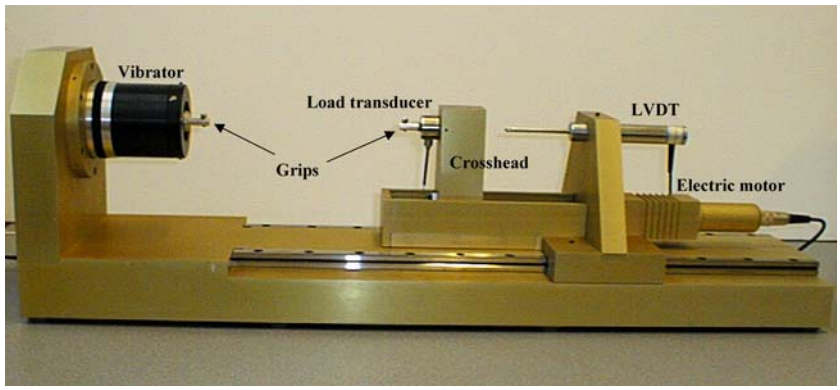

Fig. 1 The universal fibre tester

adding the one to the other so as to obtain the maximum load on the fibre. The maximum load was then maintained constant, to within ±0.1 g, by a servo system, which controlled the electric motor operating the cross-head. In this way the loading pattern on the fibre was maintained constant throughout fatigue tests, irrespective of changes in specimen length due to creep or plastic deformation. The movement of the cross-head was monitored by a LVDT (linear variable differential transformer) transducer, to within 1 μm. A controlled cyclic deformation was possible by using a Bruel and Kjaer vibrator, which operated like a loud speaker and so could be controlled precisely in amplitude and frequency. The frequency used in this study was 50 Hz, which is within the range of interest for tyre applications. Data acquisition used a PC linked to the fibre tester via a National Instrument interface card and ATS software from Sysma.

The fibre specimens were extracted manually from the bundles and glued to card supports so as to give a gauge length of 30 mm. The card protected the fibres from the machine grips.

The fibres were analysed using a variety of techniques including a Reading TA Instruments modulated differential scanning calorimeter and wide angle X-ray diffraction for which a Siemens D500 diffractometer was used in transmission mode operating at 30 kV and 8 mA (240 W). Radiation from a CoKα (λ = 0.1789 nm) was used with a Fe filter. An arrangement of slits and a collimator produced an X-ray beam with a diameter of 3 mm.

The micro-Raman spectroscopy part of the study used a ''XY'' Raman Microspectrometer (Dilor, Lille, France) equipped for signal detection with back-illuminated nitrogen-cooled Spex CCD matrices (2,000 × 256 pixels). Illumination was made with an Ar^+–Kr^+ ions laser. This instrument had a double holographic monochromator as a filter. The following excitation lines were studied (the spectral resolution (s.r.) is given): 514.5 and 647.1 nm (XY, Ar^+–Kr^+ ions laser, s.r. 0.3–1 cm^{-1}). The excitation power was kept to a few milliwatts/μm^2 measured on the sample, in order to avoid inducing any thermal effects in the fibre structure. The laser spot diameter was about 2 μm for the micro-Raman measurements in backscattering configuration with ×100 long focus Olympus MSPlan objectives (numerical aperture = 0.80). The total magnification being 1,000, the focal length was 300 mm. Because of the diabolo shape of the laser convergence along the vertical axis, the in-depth focusing in air covered about four times the XY waist (i.e. ~6 μm). Single fibres were mounted in the grips and loaded in a Universal Fibre Tester, similar to the one used for the fatigue tests, but mounted in the spectrometer. Different strain levels were applied to single fibres at a loading strain rate of 100% min^{-1}, i.e. a speed of the mobile grip of 1.6×10^{-2} s^{-1}. After stabilisation of the viscoelastic behaviour (about 5 min), i.e. stabilisation of stress versus time, Raman spectra were recorded. The range of recording times was up to about 2,700 s. The surface/core sub-structure was studied by linear scanning measurements across the fibre diameter. The laser was focused on the fibre edges and was polarised, either parallel to the fibre axis (noted //) or perpendicular (noted ⊥), by changing the alignment of the fibre with respect to the spectrometer slit.

Spectra were cleaned from plasma laser peaks and electronic pulses using, LabSpec 2.0, software (Dilor) and decomposed using two software packages: the ORIGIN software from MICROCAL™ Software, Inc (USA).

Experimental results

The as received fibres were first characterised under controlled conditions of 21 °C and 50% relative humidity. Figures 2 and 3 show the spread of fibre diameters found for each fibre, as well as the average values obtained with a total of 853 specimens of Fibre PA66-A and 572 of Fibre PA66-B. When the two histograms of diameter distribution are compared, normalised to each average diameter, it can be seen that they were similar although Fibre PA66-A showed slightly less scatter.

The stress-strain curves for each type of fibre can be seen, from Fig. 4 to be strikingly similar. They overlap, almost exactly, up to a strain of 15% beyond which Fibre PA66-B can be seen to fail at slightly higher values of stress and strain. The mechanical properties for both types of fibres are given in Table 1. The fracture morphologies of both fibres, shown in Fig. 5, were very similar and showed a region of slow crack growth, which led to the opening of the crack, due to plastic deformation and a sloping region in the failure morphology, followed by a region normal to the fibre axis which was a zone of unstable crack propagation. This type of fracture morphology has long been recognised as due to classical tensile failure [2].

The DSC results can be seen in Fig. 6. The endothermic peaks associated with fusion are at 260.1 °C for the PA66-A fibre and 254.4 °C for the PA66-B fibre (Table 2). Integration under the peaks associated with melting, allowed the enthalpy of fusion, H_f, to be calculated by comparison to the value of a perfect crystal of polyamide 66, for which a value of 196 J/g

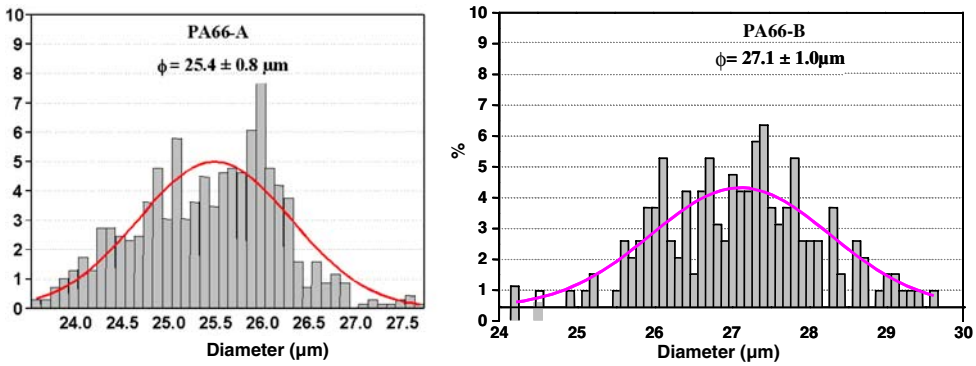

Fig. 2 Distributions of fibre diameters obtained with each type of fibre extracted from as received bundles

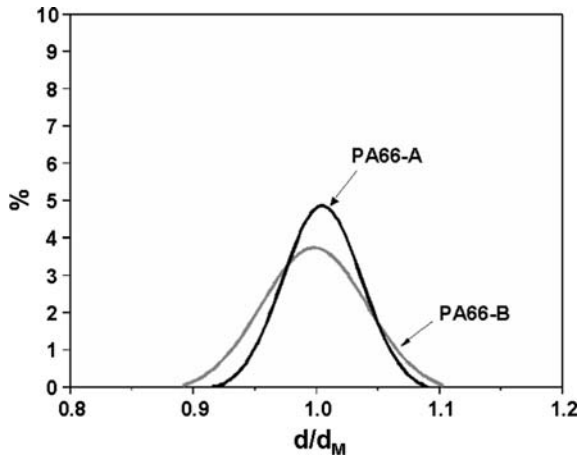

Fig. 3 The diameters of the two types of PA66 showed similar but not identical scatter when normalised to the average diameter of each type of fibre

has been determined [3]. A higher crystallinity or degree of order was revealed by DSC for the PA66-A fibre than the other but given the approximations involved, this had to be compared to the results obtained by X-ray diffraction. The values of glass transition temperature for the two types of fibres, as determined by DSC, are given in Table 3.

Table 4 shows microstructural parameters obtained by the decomposition of the X-ray diffraction spectra obtained with both types of fibres. The term ordered phase has been used in this table, rather than crystallinity, as the authors believe that this is more appropriate than suggesting an increase in the quantity of crystallinity. Loading has been seen to lead to an improvement of the molecular order and a further structuring of some of the amorphous phase, as seen by Raman spectroscopy.

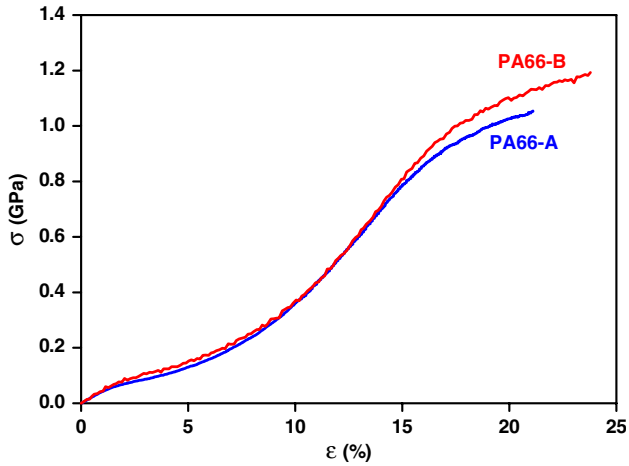

Fig. 4 The stress-strain curves of the two types of fibres

Fatigue behaviour

The fatigue tests conducted with these fibres had the initial objectives to confirm that they failed with the distinctive fracture morphology indicated in earlier publications and to determine the conditions under which fatigue occurred [4]. It has also been previously revealed that an important and necessary criterion for fatigue in this type of fibre was that the minimum load each cycle had to be lower than a threshold level [5–8]. It was hoped to further understand this condition. Based on experience from earlier studies, initial fatigue tests were conducted on the PA66-A fibres, with a minimum zero load, although care was taken to ensure that the fibre did not buckle during the test, and a maximum load equal to 60% of the simple tensile breaking load. These produced very few useful results

Table 1 Mechanical properties of the two types of polyamide 66 fibres

Fibre	No. of tests	Failure stress (GPa)	Failure strain (%)	Initial modulus (GPa)
PA66-A	33	1.10 ± 0.05	21.0 ± 1.4	4.7 ± 0.5
PA66-B	34	1.19 ± 0.06	24.0 ± 2.1	4.8 ± 0.2

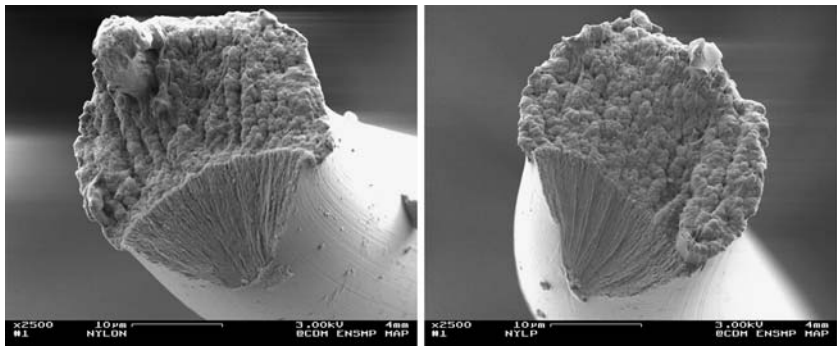

Fig. 5 Tensile fracture morphologies of PA66-A (left) and PA66-B (right)

as either failure did not occur or the fibres broke in the grips after several millions of cycles. This suggested that these high performance PA66-A fibres were significantly different from those of earlier studies, most probably due to changes in the manufacturing process. It was therefore decided to increase significantly the loading conditions on the fibres. Figure 7 shows an accumulative failure diagram for the PA666-A fibres subjected to three cyclic loading patterns corresponding to maximum loads of 75%, 80% and 85% of simple tensile strength. The dotted lines show the median values for fatigue lives under these conditions and their values are given in Table 5.

Subjecting the PA66-B fibres to similar cyclic conditions as had been used for the PA66-A fibres was found to be unsuccessful as failure occurred during the first cycle of each test. The testing conditions were progressively lowered until reasonable fatigue tests could be conducted. Figure 8 shows the accumulative failure diagram for PA66-B fibres and the dotted lines indicating the median lifetimes, under the conditions used. It should be noted that these were much lower than for the PA66-A fibres and the maximum loads

Table 2 Properties obtained by DSC

Parameter	PA66-A	PA66-B
T_f (°C)	260.1 ± 0.7	254.4 ± 1.1
H_f (J/g)	85.4 ± 5.6	80.4 ± 5.2
X_{cDSC}(%)	44 ± 2.9	41 ± 2.8

Table 3 Glass transition temperatures as evaluated from DSC results for both types of fibres

Parameter	PA66-A	PA66-B
T_g (°C)	33 ± 0.9	39.5 ± 0.7

Table 4 Structural parameters measured by X-ray diffraction

Parameter	PA66-A	PA66-B
Crystallite size	5.8 nm	5.6 nm
Ordered phase	43.5%	38.8%
Anisotropic amorphous phase	18.4%	20.2%
Isotropic amorphous phase	38.1%	41.0%
Crystallite orientation	0.972	0.976

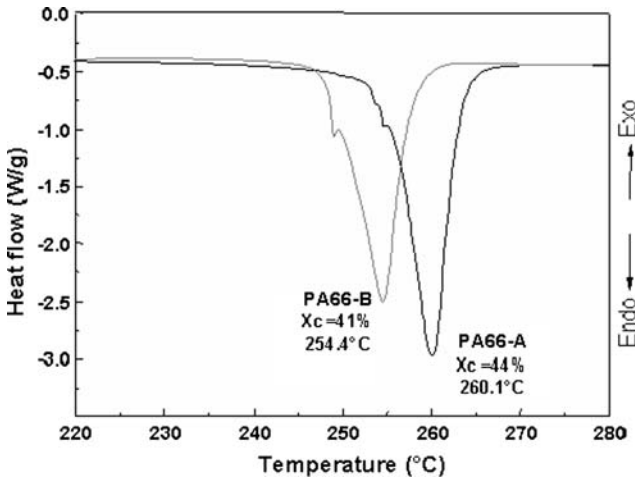

Fig. 6 DSC scans for both types of fibres

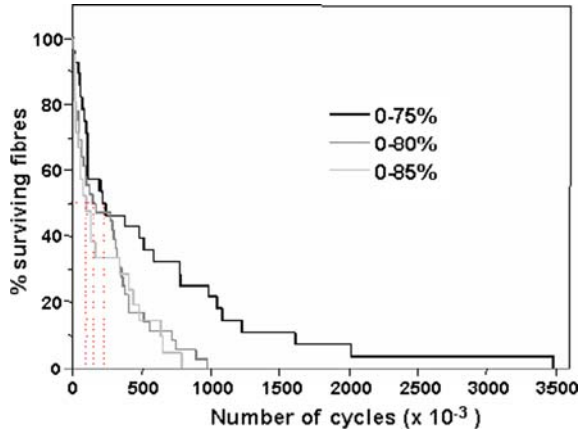

Fig. 7 Accumulative failure curves for PA66-A fibres subjected to three levels of fatigue loading indicated as percentages of simple tensile strength

Table 5 Median lifetimes for the PA66-A fibres tested at 50 Hz at 21 °C and 50% rh

Loading conditions	0–75%	0–80%	0–85%
Number of specimens tested	28	36	21
Median lifetime (cycles)	214,200	151,200	91,800
Median lifetime (hours)	1.19	0.84	0.51

Table 6 Median lifetimes for the PA66-B fibres tested at 50 Hz at 21 °C and 50% rh

Loading conditions	0–60%	0–65%	0–70%
Number of specimens tested	3	17	4
Median lifetime (cycles)	360,000	153,500	54,000
Median lifetime (hours)	2.00	0.85	0.30

corresponded to 60%, 65% and 70% simple tensile strength. These values were similar to those used in earlier studies. Table 6 shows the median lifetimes for these PA66-B fibres subjected to the three loading conditions. It can be noted that similar lifetimes were obtained when the PA66-A fibres were cycled from zero load to 80% of simple tensile strength and when the PA66-B were cycled from zero load to 65% of simple tensile strength. A comparison of the cumulative failure results of the two types of fibres broken under these conditions is given in Fig. 9. It can be seen from the dotted lines, indicating the median lifetimes that they were almost identical. Both types of fibres broke with the distinctive fatigue fracture morphologies seen in other studies [5–8]. Complementary ends of a PA66-A fibre broken in fatigue are shown in Fig. 10.

Both types of fibres were then subjected to these maximum loads but with varying minimum loads. Tables 7 and 8 give the results obtained.

The PA66-A fibres were studied by DSC and X-ray diffraction after being subjected to loading conditions (0–75% simple tensile strength) which led to fatigue. Figure 11 shows that a significant increase in the melting point was seen in the DSC results, suggesting that an increase in the perfection of the microstructure had occurred during fatigue. Figure 12 reveals that the (010), (110) doublet peak obtained by X-ray diffraction was sharper after fatigue and slightly shifted to higher

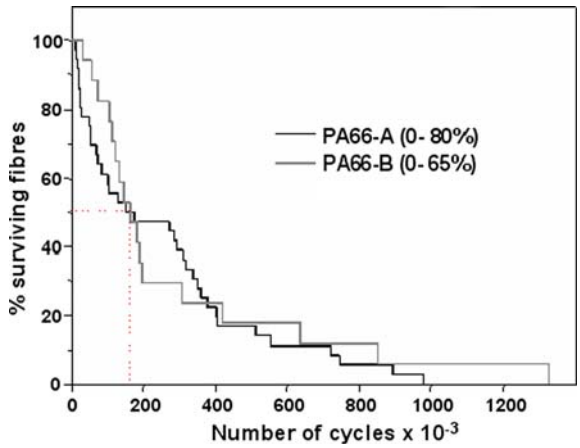

Fig. 9 A comparison of the accumulative failure curves for the PA66-A fibres, cyclically tested from zero load to 80% of tensile breaking load and the PA66-B fibres subjected to cyclic tests from zero load to 65% of simple tensile breaking load

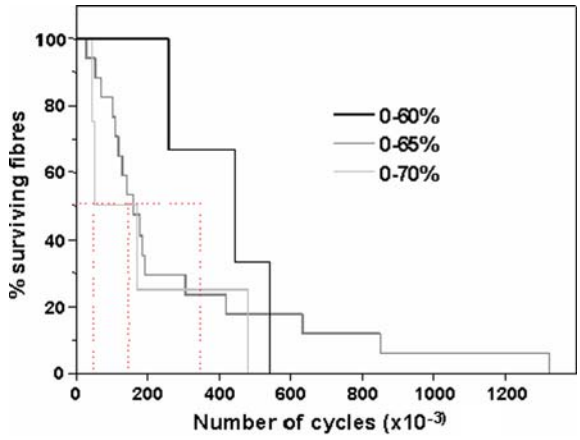

Fig. 8 Accumulative failure curves for PA66-B fibres subjected to three levels of fatigue loading indicated as percentages of simple tensile strength

Fig. 10 Complementary ends of a PA66-A fibre broken in fatigue after cycling from zero load to 80% of simple tensile strength at 50 Hz

Table 7 Median lifetimes for the PA66-A fibres cycled to 80% of simple tensile strength but with various minimum loads

Loading conditions	0–80%	5–80%	6–80%	7–80%[a]
Number of specimens tested	36	4	5	4
Median lifetime (cycles)	151,200	2.04×10^6	3.8×10^6	4.49×10^6
Median lifetime (hours)	0.84	11.33	21.11	24.94

[a] NB: the failures obtained were of the fatigue type except with the highest minimum load for which only creep type failures were obtained

angles. This has allowed an increase of about 10% in crystalline perfection to be calculated [9]. It has also shown that the anisotropic, or oriented, amorphous phase had increased, after fatigue, by 6% and that the isotropic amorphous phase had reduced by 21%.

Raman spectroscopy

A particular interest in this study was to determine the existence of any residual stresses in the fibre surface regions, which could influence their fatigue behaviours. Such residual stresses had previously been reported in similar fibres [10]. The as received fibres were held straight, but under very low load, in the fibre-testing machine, which was positioned in the Raman spectrometer. The excitation beam was then focussed on the equatorial fibre edge and scanned across it, normal to the fibre axis. In particular the low wavenumber collective modes at ~100 and ~70 cm^{-1} were considered as, respectively being representative of the crystalline and amorphous chains. The evolution of peak position revealed a variation of properties between the core and the surface regions of the fibre. Results, shown in

Table 8 Median lifetimes for the PA66-B fibres cycled to 65% of simple tensile strength but with various minimum loads

Loading conditions	0–65%	7–65%	10–65%	12–65%[a]
Number of specimens tested	17	4	4	3
Median lifetime (cycles)	153,500	1.16×10^6	5.14×10^6	6.9×10^6
Median lifetime (hours)	0.85	6.44	28.56	38.33

[a] NB: the failures obtained were of the fatigue type except with the highest minimum load for which only creep type failures were obtained

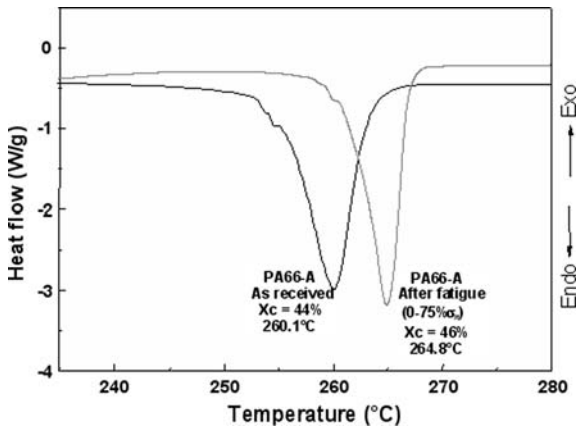

Fig. 11 DSC curves for PA66-A fibres before and after fatigue

Fig. 13a and b, confirm the differential residual stresses between the core and the surface regions of the fibre, established in previous work. Variations measured for the amorphous component was 10 times larger than that measured for the crystalline ''regions'', but opposite in sign: tensile stresses in the core for the crystalline phase and compressive stresses for the amorphous phase. The line-scan cartography provided an evaluation of sizes of the residual stress regions to be assessed and the stress state in the crystalline phase in the surface region was calculated to be between 85 and 200 MPa lower than in the fibre core. Several measurements along the fibre showed that the property gradient between surface and core appeared to vary along the fibre. A comparison of the values relating to the amorphous chains in both fibres is made in Table 9. It can be seen that the peaks associated with the amorphous phases in the surface region of both fibres were the same (65.5 $cm^{-1)}$ but that the core of fibre A

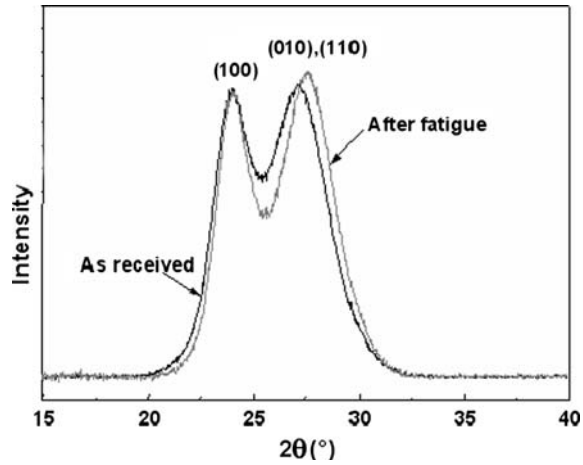

Fig. 12 X-ray diffraction peaks for the PA66-A fibre, before and after fatigue

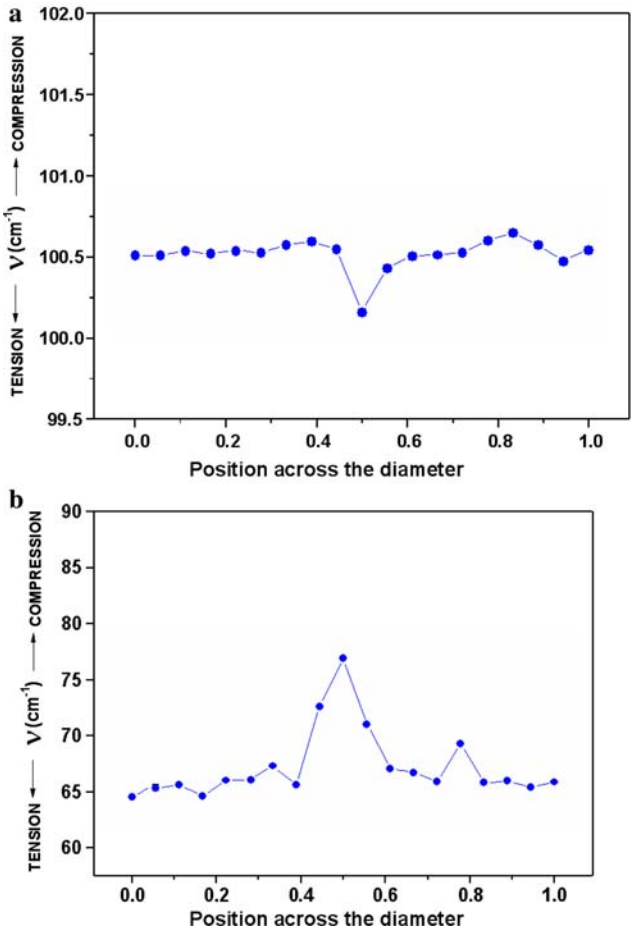

Fig. 13 (**a**) Frequency shift in the crystalline zones of a PA66-A fibres observed as the Raman excitation beam was scanned across the fibre diameter. (**b**) Wave number shift relating to the stress in amorphous regions across the diameters of three PA66-A fibres

was relatively less stressed (79.0 cm^{-1}) than that of fibre B (84.8 cm^{-1}). This means that the amorphous phase in the surface regions of fibre B was, relative to the core, more stressed than was the case for fibre A. This is shown in Table 9.

Stress experienced by chemical bonds leads to changes in interatomic distances and so changes in atomic vibration wavenumbers. This is the principle of Raman extensometry [11]. The empirical relationship between the strain-induced Raman wavenumber shift (Δv) to tensile strain ($\Delta\varepsilon$) is linear [11–18]:

$$\Delta v = S^{\varepsilon} \times \Delta^{\varepsilon} \quad (1)$$

in which S^{ε} is a coefficient expressed in $cm^{-1}/\%$ and the above equation is microscopically analogous to Hooke's law

$$\Delta v = E \times \Delta^{\varepsilon} \quad (2)$$

and

$$\Delta v = S^{\varepsilon} \times (100 \times \Delta\sigma)/E = S^{\sigma} \times \Delta\sigma \quad (3)$$

where S^{σ} is a coefficient expressed in cm^{-1}/MPa.

This expression should not be surprising as Young's modulus is a consequence, at the macroscopic scale, of the force constants of the various chemical bonds. Consequently, it has been established [19, 20] that

$$S^{\varepsilon} = k' E^{-1/2} \quad (4)$$

Following on from work previously reported for PA66 fibres [10], the variation due to straining of the amorphous and crystalline chain low wavenumber signatures of both types of fibres were studied and compared. As in the previous study, fibres were subjected to various levels of stress and strain in the Universal Fibre Tester. The deformation of the fibre was stopped and the fibre allowed to relax until the load stabilised. This took approximately 5 min. The Raman spectrum was then recorded. Very different behaviours were observed for the crystalline and amorphous signatures. The results obtained are shown in Fig. 14. Changes in the signatures can be seen to be related to different parts of the stress-strain curves of the fibres and give insights into their molecular morphologies.

The initial plateau, shown in Fig. 14 for the Raman spectroscopy results, obtained at different stresses and strains, for both crystalline and amorphous chains signatures, were consistent with an initial alignment of the chains without energy dissipation up to a threshold which differed slightly between the two fibres. The threshold for the ordered chains of the PA66-A fibres was 450 MPa, equivalent to a 11% strain whereas the equivalent values for the PA66-B fibres were 350 MPa and 10% strain. The amorphous signal reached a threshold at 500 MPa and 12% strain for the PA66-A fibres and 400 MPa and 11% strain for the PA66-B fibres. Beyond the thresholds, for both fibres, the change in wavenumber was significantly greater for the amorphous phases than for the crystalline phase. The

Table 9 Comparison of Raman signal from the amorphous phases in the skins and cores of both fibres

Fibre type	PA66- A	PA66-B
ν_{Skin} (cm^{-1})	65.5 ± 0.8	65.6 ± 1.5
ν_{Core} (cm^{-1})	79.0 ± 6.5	84.8 ± 7.3
$\Delta\nu$	13.5 ± 7.5	19.2 ± 8.8
ΔMPa	320 ± 150	1,600 ± 500

Conversion in MPa has been made using equation 3 and the values given in Table 10

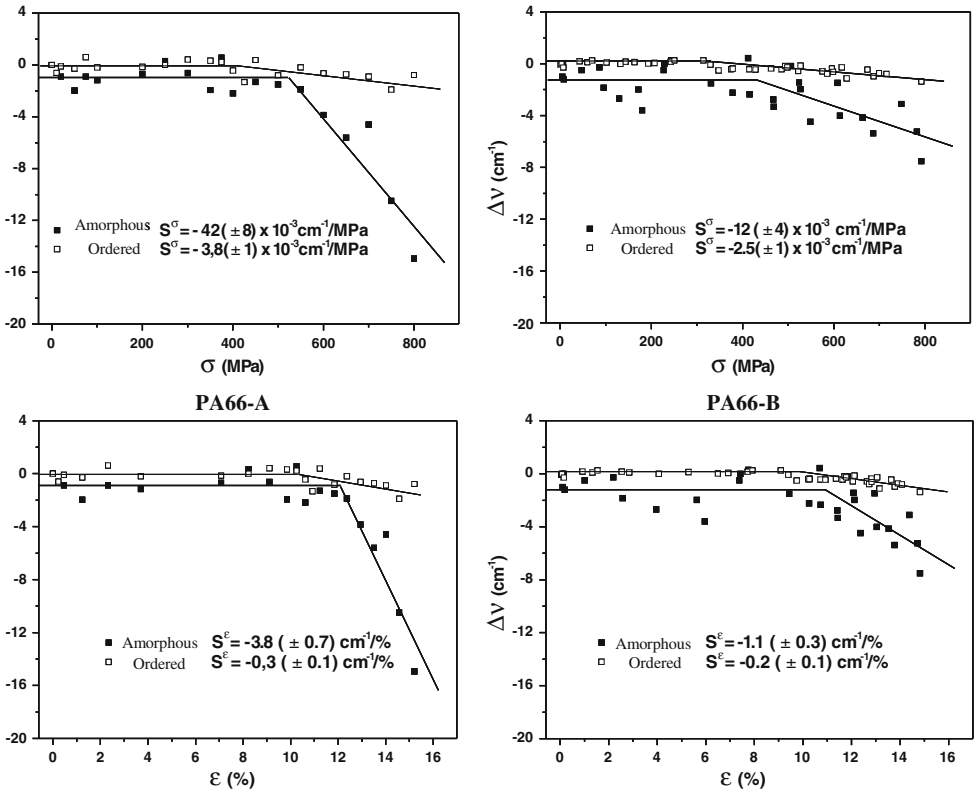

Fig. 14 Shift of the wavenumbers as measured by Raman spectroscopy for the ordered and isotropic amorphous regions in both fibres measured at different stress and stain levels

values for both $S^{\varepsilon}$and S^{σ} for the two types of fibres are shown in Table 10.

For the sake of clarity it should be noted that a decrease in wavenumber indicates an increase in bond strain, as a result of tensile forces and an increase in the value results from a decrease in the interatomic distance, resulting from compression. The coefficients S^{σ} and S^{ε} are related to the compliances of the phases and are proportional to $E^{-1/2}$. As shown in Table 10 the values of S for the amorphous phases can be seen to have differed markedly between the two fibres whereas the values for the crystalline phases were not significantly different.

Discussion

The comparison between the two types of polyamide 66 fibres has shown, very clearly, that the fatigue behaviour of such fibres cannot be predicted from their simple tensile behaviour. The two types of fibres considered in this study possessed very similar tensile properties and fracture morphologies. Both fibres had been produced for tyre cord applications, for which fatigue is an important consideration, however fibre PA66-A could be taken to 23% higher cyclic stresses than fibre PA66-B and still retained the same fatigue lifetimes.

The microstructural analyses have shown that the fibres did not share the same structural texture. Both the DSC and X-ray diffraction results show that Fibre PA66-A was the more ordered of the two. The results obtained by Raman spectroscopy reveal that the crystalline or ordered regions of both types of fibres were similar, however there were large differences between the values, shown in Table 10, for the isotropic amorphous zones revealing that in the PA66-A fibres they were less ordered and dense than in the PA66-B fibres.

Table 10 Results of Raman microextensometry for both types of fibres

Fibre	Amorphous phase		Crystalline phase	
	S^{σ}(cm^{-1}/MPa)	S^{ε} (cm^{-1}/%)	S^{σ}(cm^{-1}/MPa)	S^{ε}(cm^{-1}/%)
PA66-A	–42 (±8) × 10^{-3}	–3.8 (±0.7)	–3.8 (±1) × 10^{-3}	–0.3 (±0.1)
PA66-B	–12 (±4) × 10^{-3}	–1.1 (±0.3)	–2.5 (±1) × 10^{-3}	–0.2 (±0.1)

The crystalline perfection was seen to have been improved and the anisotropic amorphous phase had also increased to the detriment of the isotropic amorphous phase, after fatigue cycling, which illustrates that molecular movement within the body of the fibre occurred under cyclic loading.

The fatigue behaviours of the two types of fibres were qualitatively very similar but quantitatively very different. Fibre PA66-B possessed a slightly higher failure stress than Fibre PA66-A but was far inferior in fatigue. The former fibre also showed a higher minimum threshold load level for fatigue than the latter fibre. In the case of these polyamide 66 fibres the measurements of the molecular changes, occurring during loading, agree with the Prevorsek model in which the phases are in series, as shown schematically in Fig. 15. As with the fatigue model proposed by Veve et al. [21], this suggests that fatigue damage occurs throughout the body of the fibre. It is reasonable to suppose that local heating occurs due to the interaction, or friction, of the amorphous chains, which encourages their reorganisation. This accords with the observations on many tensile fracture morphologies, which suggest that melting can occur. Lowering the tensile load sufficiently, each cycle, to allow the amorphous molecules to interact and so produce heat and structural rearrangement is a likely mechanism involved in the fatigue process and explains the importance of the minimum load threshold. An earlier study has shown that fatigue initiation can occasionally occur within the fibres because of the presence of an inclusion, however observations of fatigue failures usually show crack initiation at or near the fibre surface [22]. It is tempting to conclude that the Raman spectroscopy results, which show the greater differences in stresses between the surface and the core of Fibre PA66-B compared to those in Fibre PA66-A, explain this observation. On passing under the minimum load threshold level, the amorphous regions near the fibre surface can be expected to buckle and interact and this would occur sooner with the PA66-B fibre than with the PA66-A fibre. This point could be related to differences in the cooling gradient during the process, the highest stress difference being observed for the more quenched fibre, Fibre B in this case. Figure 16 shows by how much each fibre would have to be stressed for their surfaces to experience tensile loads. The differences in surface residual stress could explain the slightly higher simple tensile strength of the PA66-B fibres, as crack initiation would be inhibited. However, the mechanism controlling the minimum load threshold level in fatigue and fatigue crack initiation could be the passage of the fibre surface regions into compression if the load each cycle

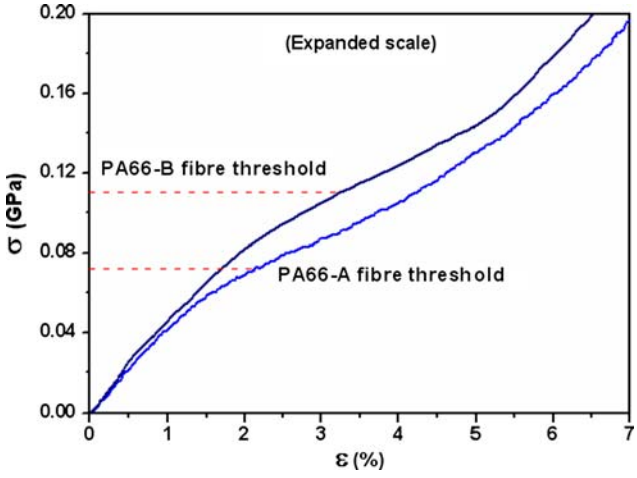

Fig. 16 The residual stress levels in the skin compared to the initial part of the tensile stress-strain curves for both types of fibres. Note the stress gap measured by Raman spectroscopy for the amorphous chains is respectively 320 and 1,600 MPa for B and A fibre, respectively

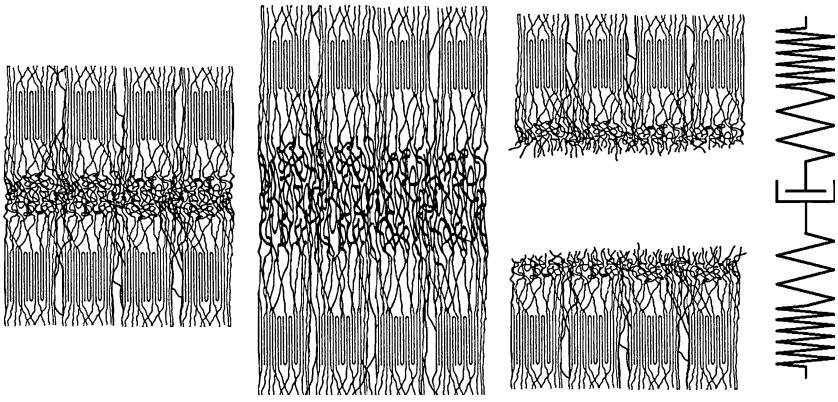

Fig. 15 Proposed structural modifications during cyclic loading of polyamide 66 fibres

is sufficiently lowered. It is recognised that crack initiation in these fibres is facilitated if they go into compression. If this is the case, it is possible that fatigue resistance could be improved by heat treatments designed to remove residual stresses in the fibres.

Conclusions

The behaviour in fatigue of polyamide fibres cannot be predicted from their simple tensile behaviour and failure. Highest strength is not necessarily an indication of best fatigue strength. It has been seen that structural changes involving changes in crystallite dimensions occur during fatigue. The study has shown considerable agreement between the mechanical characteristics of the fibres and the structural information obtained by DSC, X-ray diffraction and Raman spectroscopy. The latter technique has been of particular importance in analysing the textures of the fibres across their diameters. This could only have been achieved, using X-ray diffraction, if a synchrotron supplying a micro X-ray beam had been available. It is probable that the differences in textures between the fibres considered in the study contribute to the different fatigue behaviours. It is also possible that residual compressive stresses in the regions near the fibre surfaces, induced during fibre manufacture, may influence considerably the initiation of fatigue crack cracks and that further heat treatments may be a means of optimising fatigue behaviour.

References

1. Bunsell AR, Hearle JWS, Hunter R (1971) J Phys E 4:868
2. Hearle JWS, Lomas B, Cooke WD (1998) Atlas of fibre fracture and damage to textiles, 2nd edn. Woodhead Publishing, Oxford
3. Brandrup J, Immergut EH, Grulke EA (1999) Polymer handbook, 4th edn. J. Wiley
4. Bunsell AR, Hearle JWS (1971) J Mater Sci 6:1303
5. Bunsell AR, Hearle JWS (1974) J Appl Polym Sci 18:267
6. Oudet C, Bunsell AR (1984) J Mater Sci Lett 3: 295
7. Oudet C, Bunsell AR, Hagege R, Sotton M (1984) J Appl Polym Sci 29:4363
8. Veve JC (1987) Interprétation microstructurale de l'endommagement par fatigue mécanique des fibres de polyester pour le renforcement des élastomères. PhD thesis, Ecole des Mines de Paris
9. Haberkorn H, Illers KH, Simak P (1979) Polym Bull 1:485
10. Marcellan A, Bunsell AR, Piques R, Colomban P (2003) J Mater Sci 38:2117
11. Colomban Ph (2002) Adv Eng Mater 4:535
12. Herrera Ramirez JM, Colomban Ph, Bunsell A (2004) Proc. Polymer Fibres 2004, UMIST Conference Centre, Manchester, UK
13. Kitagawa T, Ishitobi M, Yabuki K (2000) J Polym Sci Polym Phys 38:1605
14. Young RJ, Yeh WY (1994) Polymer 35:3844
15. Young RJ (1994) Raman Spectroscopy and mechanical properties. In: Spells SJ (eds) Characterization of solid polymers. Chapman & Hall, London, p 224
16. Beyerlein IJ, Amer MS, Schadler LS, Phoenix SL (1998) Sci Eng Comp Mater 7(1–2):151
17. Yeh W-Y, Young RJ (1998) J Macromol Sci Phys 37:83
18. Yeh W-Y, Young RJ (1999) Polymer 40:857
19. Gouadec G, Colomban Ph (2001) J Eur Ceram Soc 21:1249
20. Gouadec G, Colomban Ph (2007) Progr Cryst Growth Character 53(1–2)
21. Veve JC, Bunsell AR, Baillie C, Hagege R (1987) Kautschuk Gummi Kunstoffe 40:941
22. Herrera Ramirez JM, Bunsell AR (2005) J Mater Sci 40:1269